

# Enhanced Latent Multi-view Subspace Clustering

Long Shi, *Member, IEEE*, Lei Cao, Jun Wang, Badong Chen, *Senior Member, IEEE*

**Abstract**—Latent multi-view subspace clustering has been demonstrated to have desirable clustering performance. However, the original latent representation method vertically concatenates the data matrices from multiple views into a single matrix along the direction of dimensionality to recover the latent representation matrix, which may result in an incomplete information recovery. To fully recover the latent space representation, we in this paper propose an Enhanced Latent Multi-view Subspace Clustering (ELMSC) method. The ELMSC method involves constructing an augmented data matrix that enhances the representation of multi-view data. Specifically, we stack the data matrices from various views into the block-diagonal locations of the augmented matrix to exploit the complementary information. Meanwhile, the non-block-diagonal entries are composed based on the similarity between different views to capture the consistent information. In addition, we enforce a sparse regularization for the non-diagonal blocks of the augmented self-representation matrix to avoid redundant calculations of consistency information. Finally, a novel iterative algorithm based on the framework of Alternating Direction Method of Multipliers (ADMM) is developed to solve the optimization problem for ELMSC. Extensive experiments on real-world datasets demonstrate that our proposed ELMSC is able to achieve higher clustering performance than some state-of-art multi-view clustering methods.

**Index Terms**—ADMM, complementary information, consistent information, latent representation, multi-view subspace clustering, sparse regularization.

## I. INTRODUCTION

Subspace clustering for dealing with high-dimensional data has emerged as a research focus in the field of computer vision over the past decade, offering significant success in diverse scenarios including face clustering [1], [2], [3], motion segmentation [4], [5], handwritten character recognition [6], [7]. However, when confronted with insufficient or noisy data observations, subspace clustering inevitably experiences significant deterioration. This is because subspace clustering is essentially a single-view clustering technique, which is not tolerant of low-quality view data [8]. To address this challenge, multi-view clustering has arisen as a powerful solution that exploits abundant data sources from diverse domains [9], [10].

Long Shi and Lei Cao are with the School of Computing and Artificial Intelligence, and also with the Financial Intelligence and Financial Engineering Key Laboratory of Sichuan Province, Southwestern University of Finance and Economics, Chengdu 611130, China (e-mail: shilong@swufe.edu.cn, caolei2000@smail.swufe.edu.cn). These two authors contributed equally to this work.

Jun Wang is with the School of Management Science and Engineering, Southwestern University of Finance and Economics, Chengdu 611130, China (e-mail: wangjun1987@swufe.edu.cn).

Badong Chen is with the Institute of Artificial Intelligence and Robotics, Xi'an Jiaotong University, Xi'an 710049, China (e-mail: chenbd@mail.xjtu.edu.cn).

The work of Long Shi was partially supported by the National Natural Science Foundation of China under Grant 62201475. The work of Badong Chen was supported by the National Natural Science Foundation of China under Grants U21A20485 and 61976175.

The concept of multi-view stems from intuitive observations made in various practical scenarios. For instance, in the context of web page products, each product page comprises textual descriptions, product images, and user engagement data. Unlike conventional subspace clustering, the multi-view clustering approach can demonstrate impressive performance even in the presence of limited-quality view data [11], [12].

Graph-based methods hold an important position in the field of multi-view clustering [13], [14], [15], primarily owing to the intrinsic capacity of graphs to capture and utilize relationships between data points across various views. In [13], the authors introduced a co-regularization framework for multi-view spectral clustering to align clustering hypotheses. [16] proposed a multiview consensus graph clustering method by defining an effective cost function for disagreement measure and imposing a rank constraint on the Laplacian matrix. [17] suggested integrating the shared affinity matrix learning stage and the  $k$ -means clustering stage in a framework. To attain a parameter-free clustering model, [18] developed a multi-view extension of spectral rotation with procrustes average. Multiple kernel learning has been acknowledged as another important technique for multi-view clustering. [19] proposed a multiple kernel  $k$ -means clustering method with a matrix-induced regularization to improve the diversity of the selected kernels. With late fusion alignment maximization, [20] proposed an effective clustering method to reduce the computational cost and simplify the optimization procedures. For more advanced graph-based and multiple kernel clustering methods, readers are encouraged to refer [21], [22], [23], [24], [25], [26].

In addition to the previously mentioned methods, multi-view subspace clustering has also gained significant popularity. [10] performed subspace clustering on each view while ensuring the coherence of the clustering structure among different views. [27] enforced the multi-view subspace clustering with low-rank and sparse structures. In order to comprehensively explore the underlying data distribution across distinct views, [28] proposed a subspace learning method that simultaneously takes consistency and diversity into account. Motivated by the underlying assumption that multiple views are generated from one shared latent representation, the latent representation-based multi-view subspace clustering methods have garnered much attention [29], [30], [31]. In contrast to conventional multi-view subspace clustering methods, the latent representation method first recovers the latent space matrix, followed by the learning of the self-representation matrix based on the derived latent representation matrix. Despite the promising results achieved, the existing latent representation-based methods directly concatenate the data matrices from multiple views into a single matrix along the direction of dimensionality. This data concatenation strategy only takes into account the unique information from each view, and fails to exploit the similarity,

also known as consistency, between different views, thereby limiting its ability to facilitate a comprehensive recovery of the latent representation matrix.

To this end, we propose a novel latent representation clustering method called Enhanced Latent Multi-view Subspace Clustering (ELMSC). We take into account the complementarity and consistency of various views simultaneously to construct an augmented multi-view data matrix, which is useful for learning an exhaustive latent representation matrix. For the purpose of concept alignment, we refer to the latent representation in this paper as the augmented latent representation matrix. Our main contributions include:

- To guarantee the complementary information of each view as well as exploit the consistent information across views, we construct an augmented data matrix, in which the block-diagonal locations stack the data matrices from different views and the non-block-diagonal entries consist of the similarity information between different views.
- We enforce a sparse regularization for the non-diagonal blocks of the augmented self-representation matrix to avoid redundant calculations of consistent information between different views. It is worth noting this regularization does not affect the diagonal blocks, ensuring the preservation of complete complementary information.
- An iterative optimization algorithm is developed to solve the optimization problem for ELMSC by using the framework of Alternating Direction Method of Multipliers (ADMM) [32].
- We establish the relationship between the traditional latent multi-view technique and our method under some specific conditions, indicating that our approach can be regarded as an augmented variant of the traditional method.

Experiments on six real-world datasets have demonstrated that the proposed ELMSC method outperforms some advanced multi-view clustering methods. Moreover, our method is not significantly sensitive to parameter selection, and it can still achieve satisfactory performance even when parameters are selected randomly.

## II. PRELIMINARIES

### A. Multi-view Subspace Clustering

Multi-view Subspace Clustering (MVSC) [10] aims to address the limitations of traditional subspace clustering methods by combining information from diverse sources to reveal underlying structures and relationships. Consider multi-view data  $\{\mathbf{X}^{(l)}\}_{l=1}^v$ , where  $\mathbf{X}^{(l)} \in \mathbb{R}^{d_l \times n}$  denotes the  $l$ -th view data with  $d_l$  dimensions. The objective optimization problem of MVSC can be defined as

$$\begin{aligned} \min_{\mathbf{Z}^{(l)}, \mathbf{Z}} \sum_l \|\mathbf{X}^{(l)} - \mathbf{X}^{(l)}\mathbf{Z}^{(l)}\|_F^2 + \lambda f(\mathbf{Z}, \mathbf{Z}^{(l)}), \\ \text{s.t. } \mathbf{Z}_l \geq 0, (\mathbf{Z}^{(l)})^T \mathbf{1} = \mathbf{1}, \end{aligned} \quad (1)$$

where  $\|\cdot\|_F$  represents the  $F$ -norm,  $\mathbf{Z}^{(l)} \in \mathbb{R}^{n \times n}$  denotes the non-negative self-representation matrix,  $\mathbf{Z}$  accounts for the unified self-representation matrix,  $\lambda$  is a balance parameter,

and  $f(\cdot)$  represents the unified regularization term. The equation  $(\mathbf{Z}^{(l)})^T \mathbf{1} = \mathbf{1}$  enforces the constraint that the coefficients of data points within a subspace should sum up to 1, ensuring that the data points are fully represented within their respective subspaces during the clustering process.

After acquiring the unified self-representation matrix  $\mathbf{Z}$ , the subsequent procedure is to perform spectral clustering to obtain the ultimate clustering results. This process involves the construction of the affinity matrix via  $\mathbf{W} = \frac{|\mathbf{Z}| + |\mathbf{Z}^T|}{2}$ , followed by the resolution of an optimization problem

$$\min_{\mathbf{F}} \text{Tr}(\mathbf{F}^T \mathbf{L} \mathbf{F}), \text{ s.t. } \mathbf{F}^T \mathbf{F} = \mathbf{I}, \quad (2)$$

where  $\text{Tr}(\cdot)$  takes the trace of a matrix,  $\mathbf{L} = \mathbf{D} - \mathbf{W}$  is the Laplacian matrix with diagonal matrix defined as  $d_{ii} = \sum_{j=1}^n z_{ij}$  [33], and  $\mathbf{F}$  is the cluster indicator matrix.

### B. Latent Multi-view Subspace Clustering

In Latent Multi-view Subspace Clustering (LMSC) [29], the self-representation matrix is learned from the recovered latent space representation, in contrast to the conventional multi-view subspace clustering methods that rely on data representations. The objective optimization of LMSC is formulated as

$$\begin{aligned} \min_{\mathbf{P}, \mathbf{H}, \mathbf{Z}} f_h(\mathbf{X}, \mathbf{P}\mathbf{H}) + \lambda_1 f_r(\mathbf{H}, \mathbf{H}\mathbf{Z}) + \lambda_2 \Omega(\mathbf{Z}) \\ \text{with } \mathbf{X} = \begin{bmatrix} \mathbf{X}^{(1)} \\ \dots \\ \mathbf{X}^{(v)} \end{bmatrix} \text{ and } \mathbf{P} = \begin{bmatrix} \mathbf{P}^{(1)} \\ \dots \\ \mathbf{P}^{(v)} \end{bmatrix}, \end{aligned} \quad (3)$$

where  $\mathbf{X} \in \mathbb{R}^{d \times n}$  denotes the reconstruction data matrix with  $d = \sum_l d_l$ ,  $\mathbf{P} \in \mathbb{R}^{d \times k}$  is the projection matrix,  $\mathbf{H} \in \mathbb{R}^{k \times n}$  represents the latent representation matrix,  $\mathbf{Z}$  is the self-representation matrix also known as the reconstruction coefficient matrix,  $\lambda_1$  and  $\lambda_2$  are the balance parameters. The function  $f_h(\mathbf{X}, \mathbf{P}\mathbf{H})$  serves to recover the underlying latent representation  $\mathbf{H}$ ,  $f_r(\mathbf{H}, \mathbf{H}\mathbf{Z})$  is used to learn the self-representation matrix  $\mathbf{Z}$ , and  $\Omega(\mathbf{Z})$  is a regularization term.

## III. PROPOSED METHODOLOGY

In this section, we will comprehensively introduce the proposed ELMSC methodology, offering a detailed presentation of its motivation, formulation, optimization procedures, and an analysis of its computational complexity. The framework of ELMSC is shown in Fig. 1.

### A. Motivation

As shown in (3), conventional multi-view subspace clustering methods vertically concatenate the data matrix of each view to form a multi-view matrix for latent representation learning. While this construction method captures the inherent complementarity across diverse views, it lacks the capability to exploit the consistent information between views. Thus, there arises a need to devise a more effective multi-view data matrix construction strategy to enhance representation quality, thereby facilitating the recovery of an improved latent representation. The motivation of our paper will be further emphasized towards the end of the Problem Formulation subsection, through a comparison between the conventional data reconstruction method and our approach.

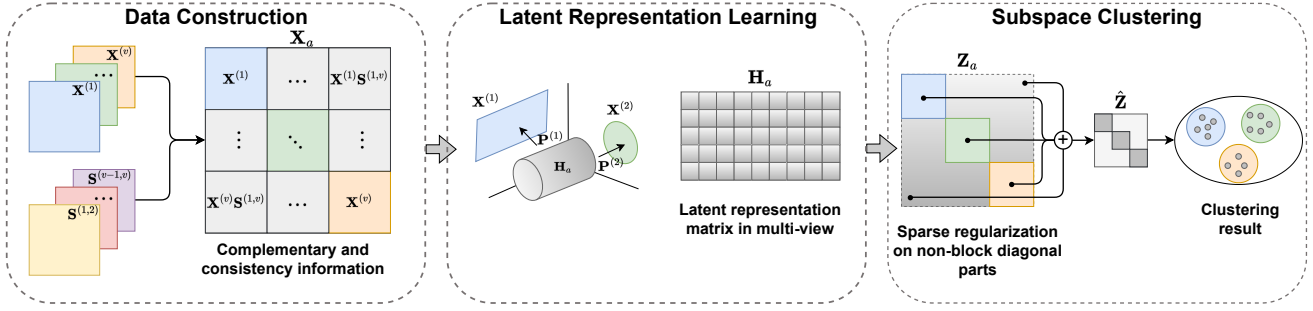


Fig. 1: Framework of ELMSC.

### B. Problem Formulation

In order to enhance the multi-view data representation, we define an augmented data matrix  $\mathbf{X}_a$ , in which the block-diagonal locations stack the data matrices from different views to preserve the complementary information, while the non-block-diagonal regions contain inter-view similarities to capture the consistent information. Specifically, the augmented data matrix  $\mathbf{X}_a \in \mathbb{R}^{d \times vn}$  takes the form

$$\mathbf{X}_a = \begin{bmatrix} \mathbf{X}^{(1)} & \mathbf{X}^{(1,2)} & \dots & \mathbf{X}^{(1,v)} \\ \mathbf{X}^{(2,1)} & \mathbf{X}^{(2)} & \dots & \mathbf{X}^{(2,v)} \\ \vdots & \vdots & \ddots & \vdots \\ \mathbf{X}^{(v,1)} & \mathbf{X}^{(v,2)} & \dots & \mathbf{X}^{(v)} \end{bmatrix}, \quad (4)$$

where  $\mathbf{X}^{(p,q)} \in \mathbb{R}^{d_p \times n}$  denotes the correlation matrix between the  $p$ -th and  $q$ -th views that is calculated by

$$\mathbf{X}^{(p,q)} = \mathbf{X}^{(p)} \mathbf{S}^{(p,q)}, \text{ for } p \neq q. \quad (5)$$

In (5),  $\mathbf{S}^{(p,q)}$  represents the cosine similarity matrix [34] with its element  $S_{i,j}^{(p,q)}$  computed by

$$S_{i,j}^{(p,q)} = \frac{\tilde{\mathbf{X}}_{:,i}^{(p)} \cdot \tilde{\mathbf{X}}_{:,j}^{(q)}}{2 \|\tilde{\mathbf{X}}_{:,i}^{(p)}\|_2 \|\tilde{\mathbf{X}}_{:,j}^{(q)}\|_2} + \frac{1}{2}, \quad (6)$$

where  $\tilde{\mathbf{X}}^{(p)}$  and  $\tilde{\mathbf{X}}^{(q)}$  are the data matrices after dimensionality reduction via Principal Component Analysis (PCA) [35], [36], a procedure aimed at aligning data dimensions between the  $p$ -th and  $q$ -th views. Further details on the implementation of PCA will be illustrated in the section of Experiments. This alignment is essential in enabling the computation of cosine similarity. The symbols  $\tilde{\mathbf{X}}_{:,i}^{(p)}$  and  $\tilde{\mathbf{X}}_{:,j}^{(q)}$  denote the  $i$ -th row and the  $j$ -th row of  $\tilde{\mathbf{X}}^{(p)}$  and  $\tilde{\mathbf{X}}^{(q)}$ , respectively.  $\tilde{\mathbf{X}}_{:,i}^{(p)} \cdot \tilde{\mathbf{X}}_{:,j}^{(q)}$  calculates the inner product of two vectors. From (6), it is evident to infer that  $0 \leq S_{i,j}^{(p,q)} \leq 1$  and  $\mathbf{S}^{(p,q)} = \mathbf{S}^{(q,p)}$ .

Subsequently, we focus on the formulation of the objective optimization problem. First, the objective function for learning the underlying latent representation is defined as follows

$$\min_{\mathbf{P}, \mathbf{H}_a} J_1(\mathbf{X}_a, \mathbf{P}\mathbf{H}_a), \quad (7)$$

where  $\mathbf{H}_a \in \mathbb{R}^{k \times vn}$  denotes the augmented latent representation matrix, and  $J_1(\cdot)$  is the loss function associated with the latent presentation. It is worth noting that in contrast to the objective function concerning latent representation in LMSC, as shown in (3), the constructed multi-view data matrix  $\mathbf{X}_a$

and the latent representation matrix  $\mathbf{H}_a$  in our method undergo augmentation in the formulation, which is expected to offer enhanced representation capabilities.

Then, with the latent representation matrix in (7), the objective function of self-representation based subspace clustering is formulated as

$$\min_{\mathbf{Z}_a} J_2(\mathbf{H}_a, \mathbf{H}_a \mathbf{Z}_a) + \text{Reg}(\mathbf{Z}_a), \quad (8)$$

where  $\mathbf{Z}_a \in \mathbb{R}^{vn \times vn}$  denotes the augmented self-representation matrix,  $J_2(\cdot)$  is the loss function associated with the data self-representation, and  $\text{Reg}(\cdot)$  stands for a regularization term.

To learn the augmented self-representation matrix based on the recovered latent representation, we combine (7) with (8), and arrive at

$$\min_{\mathbf{P}, \mathbf{H}_a, \mathbf{Z}_a} J_1(\mathbf{X}_a, \mathbf{P}\mathbf{H}_a) + \lambda_1 J_2(\mathbf{H}_a, \mathbf{H}_a \mathbf{Z}_a) + \lambda_2 \text{Reg}(\mathbf{Z}_a), \quad (9)$$

where  $\lambda_1$  and  $\lambda_2$  are constants used for balancing the terms. For the purpose of avoiding redundant calculations of consistent information between different views, we consider enforcing a sparse regularization for the non-diagonal blocks of  $\mathbf{Z}_a$ . Simultaneously, to ensure the algorithm's robustness against outliers, the final objective function is presented as follows

$$\begin{aligned} & \min_{\mathbf{P}, \mathbf{H}_a, \mathbf{Z}_a, \mathbf{E}_1, \mathbf{E}_2} \|\mathbf{E}_1\|_{2,1} + \lambda_1 \|\mathbf{E}_2\|_{2,1} + \lambda_2 \|\mathbf{Z}_a - \text{diag}(\mathbf{Z}_a)\|_1 \\ & \text{s.t. } \mathbf{X}_a = \mathbf{P}\mathbf{H}_a + \mathbf{E}_1, \mathbf{H}_a = \mathbf{H}_a \mathbf{Z}_a + \mathbf{E}_2, \mathbf{P}\mathbf{P}^T = \mathbf{I}, \end{aligned} \quad (10)$$

where  $\mathbf{E}_1, \mathbf{E}_2$  are the error matrices,  $\|\cdot\|_{2,1}$  and  $\|\cdot\|_1$  perform the  $l_{2,1}$ -norm and  $l_1$ -norm operations, respectively. Alternatively, by stacking  $\mathbf{E}_1$  and  $\mathbf{E}_2$  into an integrated error matrix, the objective function in (10) can be written into a compact form

$$\begin{aligned} & \min_{\mathbf{P}, \mathbf{H}_a, \mathbf{Z}_a, \mathbf{E}_1, \mathbf{E}_2} \|\mathbf{E}\|_{2,1} + \lambda \|\mathbf{Z}_a - \text{diag}(\mathbf{Z}_a)\|_1 \\ & \text{s.t. } \mathbf{X}_a = \mathbf{P}\mathbf{H}_a + \mathbf{E}_1, \mathbf{H}_a = \mathbf{H}_a \mathbf{Z}_a + \mathbf{E}_2, \\ & \mathbf{E} = [\mathbf{E}_1; \mathbf{E}_2], \mathbf{P}\mathbf{P}^T = \mathbf{I}, \end{aligned} \quad (11)$$

where  $\lambda$  is a positive balance parameter.

**Remark 1:** It is seen from (3) that the LMSC method directly concatenates the data matrices from multiple views into a single matrix along the direction of dimensionality. In this approach, only the unique information from each view  $\mathbf{X}^{(l)}$ , often referred to as complementary information, is utilized, while shared information, also known as consistent

information, is neglected. In contrast, our method arranges the data matrices from different views within the block-diagonal segments, with the non-block-diagonal regions stacked by the correlation matrix  $\mathbf{X}^{(p,q)}$  to capture inter-view similarities. Our proposed formulation can simultaneously exploit both complementarity and consistency for a more comprehensive latent representation recovery.

### C. Optimization

To solve the optimization problem in (11), we employ ADMM which is a widely used method known as the Augmented Lagrange Multiplier (ALM) with Alternating Direction Minimizing (ADM) strategy [37], which is suitable for addressing multivariate constrained optimization problems. The basic idea of ADM is to solve each variable induced subproblem by maintaining the other variables fixed. Before further proceeding, we need to introduce an auxiliary variable to make our cost function separable. In particular, we use  $\mathbf{J}$  to replace  $\mathbf{Z}_a$  in the sparse regularization term, yielding

$$\begin{aligned} & \min_{\mathbf{P}, \mathbf{H}_a, \mathbf{Z}_a, \mathbf{J}, \mathbf{E}_1, \mathbf{E}_2} \|\mathbf{E}\|_{2,1} + \lambda \|\mathbf{J} - \text{diag}(\mathbf{J})\|_1 \\ & \text{s.t. } \mathbf{X} = \mathbf{P}\mathbf{H}_a + \mathbf{E}_1, \mathbf{H}_a = \mathbf{H}_a\mathbf{Z}_a + \mathbf{E}_2, \\ & \mathbf{E} = [\mathbf{E}_1; \mathbf{E}_2], \mathbf{P}\mathbf{P}^T = \mathbf{I}, \mathbf{J} = \mathbf{Z}_a. \end{aligned} \quad (12)$$

With the ALM method, we have from (12)

$$\begin{aligned} & \mathcal{L}(\mathbf{P}, \mathbf{H}_a, \mathbf{Z}_a, \mathbf{E}_1, \mathbf{E}_2, \mathbf{J}) \\ & = \|\mathbf{E}\|_{2,1} + \lambda \|\mathbf{J} - \text{diag}(\mathbf{J})\|_1 + \Phi(\mathbf{Y}_1, \mathbf{X}_a - \mathbf{P}\mathbf{H}_a - \mathbf{E}_1) \\ & \quad + \Phi(\mathbf{Y}_2, \mathbf{H}_a - \mathbf{H}_a\mathbf{Z}_a - \mathbf{E}_2) + \Phi(\mathbf{Y}_3, \mathbf{J} - \mathbf{Z}_a) \\ & \text{s.t. } \mathbf{P}\mathbf{P}^T = \mathbf{I}, \end{aligned} \quad (13)$$

where  $\Phi(\Theta, \Psi) = \frac{\mu}{2} \|\Psi\|_F^2 + \text{Tr}(\Theta^T \Psi)$  with  $\mu$  being a positive value,  $\mathbf{Y}_1$ ,  $\mathbf{Y}_2$  and  $\mathbf{Y}_3$  are Lagrange multipliers. To solve (13), we decompose our problem into the subsequent subproblems.

#### 1) P-subproblem

To update  $\mathbf{P}$ , we treat  $\mathbf{P}$  as a variable while maintaining the other variables fixed, leading to

$$\begin{aligned} & \mathbf{P}^* = \arg \min \Phi(\mathbf{Y}_1, \mathbf{X}_a - \mathbf{P}\mathbf{H}_a - \mathbf{E}_1) \\ & \text{s.t. } \mathbf{P}\mathbf{P}^T = \mathbf{I}. \end{aligned} \quad (14)$$

The objective optimization in (14) can be equivalently transformed into

$$\begin{aligned} & \mathbf{P}^* = \arg \min \frac{\mu}{2} \|\mathbf{X}_a - \mathbf{P}\mathbf{H}_a - \mathbf{E}_1 + \mathbf{Y}_1\|_F^2 \\ & = \arg \min \frac{\mu}{2} \|(\mathbf{X}_a + \mathbf{Y}_1/\mu - \mathbf{E}_1) - \mathbf{P}\mathbf{H}_a\|_F^2 \\ & = \arg \min \frac{\mu}{2} \|(\mathbf{X}_a\mathbf{Y}_1/\mu - \mathbf{E}_1)^T - \mathbf{H}_a^T\mathbf{P}^T\|_F^2. \end{aligned} \quad (15)$$

To further proceed with (15), it is necessary to present the following theorem.

**Theorem 1** [38]: For the objective function  $\min_{\Gamma} \|\Upsilon - \Xi\Gamma\|_F^2$  s.t.  $\Gamma^T\Gamma = \Gamma\Gamma^T = \mathbf{I}$ , the optimal solution is  $\Gamma = \mathbf{U}\mathbf{V}^T$ , where  $\mathbf{U}$  and  $\mathbf{V}$  are left and right singular values of SVD decomposition of  $\Xi^T\Upsilon$ .

According to the above theorem, it is not difficult to derive that the solution to (15) is  $\mathbf{P}^T = \mathbf{U}\mathbf{V}^T$ , where  $\mathbf{U}$  and  $\mathbf{V}$  is

the left and right singular values of SVD of  $\mathbf{H}_a(\mathbf{Y}_1/\mu + \mathbf{X}_a - \mathbf{E}_1)^T$ .

#### 2) H<sub>a</sub>-subproblem

To update  $\mathbf{H}_a$ , we treat  $\mathbf{H}_a$  as a variable while keeping the other variables fixed, resulting in

$$\begin{aligned} & \mathbf{H}_a^* = \arg \min \Phi(\mathbf{Y}_1, \mathbf{X}_a - \mathbf{P}\mathbf{H}_a - \mathbf{E}_1) \\ & \quad + \Phi(\mathbf{Y}_2, \mathbf{H}_a - \mathbf{H}_a\mathbf{Z}_a - \mathbf{E}_2). \end{aligned} \quad (16)$$

Taking the derivative with respect to  $\mathbf{H}_a$  and setting the resulted equation to zero, we arrive at

$$\begin{aligned} & \mathbf{A}\mathbf{H}_a + \mathbf{H}_a\mathbf{B} = \mathbf{C} \\ & \text{with } \mathbf{A} = \mu\mathbf{P}^T\mathbf{P}, \\ & \mathbf{B} = \mu(\mathbf{Z}_a\mathbf{Z}_a^T - \mathbf{Z}_a - \mathbf{Z}_a^T + \mathbf{I}), \\ & \mathbf{C} = \mathbf{P}^T\mathbf{Y}_1 + \mathbf{Y}_2(\mathbf{Z}_a^T - \mathbf{I}) \\ & \quad + \mu(\mathbf{P}^T\mathbf{X}_a + \mathbf{E}_2^T - \mathbf{P}^T\mathbf{E}_1 - \mathbf{E}_2\mathbf{Z}_a^T). \end{aligned} \quad (17)$$

The equation presented above is a Sylvester equation, and it can be effectively solved using the ‘‘lyap’’ function in MATLAB.

#### 3) Z<sub>a</sub>-subproblem

Upon fixing the other variables, we update  $\mathbf{Z}_a$  by solving the following objective optimization problem

$$\begin{aligned} & \mathbf{Z}_a^* = \arg \min \Phi(\mathbf{Y}_3, \mathbf{J} - \mathbf{Z}_a) + \Phi(\mathbf{Y}_2, \mathbf{H}_a - \mathbf{H}_a\mathbf{Z}_a - \mathbf{E}_2). \end{aligned} \quad (18)$$

By taking the derivative with respect to  $\mathbf{Z}_a$  and setting the resulted equation to zero, we obtain

$$\begin{aligned} & \mathbf{Z}_a^* = (\mathbf{H}_a^T\mathbf{H}_a + \mathbf{I})^{-1} \\ & \quad [(\mathbf{J} + \mathbf{H}_a^T\mathbf{H}_a - \mathbf{H}_a^T\mathbf{E}_2) + (\mathbf{Y}_3 + \mathbf{H}_a^T\mathbf{Y}_2)/\mu]. \end{aligned} \quad (19)$$

#### 4) E-subproblem

Under the condition of fixing other variables, the error matrix  $\mathbf{E}$  is updated by solving the following problem

$$\begin{aligned} & \mathbf{E}^* = \arg \min \|\mathbf{E}\|_{2,1} + \Phi(\mathbf{Y}_1, \mathbf{X}_a - \mathbf{P}\mathbf{H}_a - \mathbf{E}_1) \\ & \quad + \Phi(\mathbf{Y}_2, \mathbf{H}_a - \mathbf{H}_a\mathbf{Z}_a - \mathbf{E}_2) \\ & = \frac{1}{\mu} \|\mathbf{E}\|_{2,1} + \frac{1}{2} \|\mathbf{E} - \mathbf{G}\|_F^2, \end{aligned} \quad (20)$$

where  $\mathbf{G} = [\mathbf{X}_a - \mathbf{P}\mathbf{H}_a + \mathbf{Y}_1/\mu; \mathbf{H}_a - \mathbf{H}_a\mathbf{Z}_a + \mathbf{Y}_2/\mu]$ . This subproblem can be effectively solved by using Lemma 4.1 in [6].

#### 5) J-subproblem

Following a similar approach, we update  $\mathbf{J}$  by solving the following optimization problem

$$\begin{aligned} & \mathbf{J}^* = \arg \min \lambda \|\mathbf{J} - \text{diag}(\mathbf{J})\|_1 + \Phi(\mathbf{Y}_3, \mathbf{J} - \mathbf{Z}_a) \\ & = \arg \min \frac{\lambda}{\mu} \|\mathbf{J} - \text{diag}(\mathbf{J})\|_1 + \frac{1}{2} \|\mathbf{J} - (\mathbf{Z}_a - \mathbf{Y}_3/\mu)\|_F^2. \end{aligned} \quad (21)$$

By using the singular value thresholding operator [39], the update on  $\mathbf{J}$  has a closed-form solution given by

$$\begin{aligned} & \mathbf{J}^* = \mathbf{J}_1 + \mathbf{J}_2 \\ & \text{with } \mathbf{J}_1 = \text{blkdiag}(\mathbf{J}) \\ & \mathbf{J}_2 = \mathcal{T}_{\frac{\lambda}{\mu}}(\mathbf{J} - \mathbf{J}_1) \\ & \mathbf{J} = \mathbf{Z}_a - \mathbf{Y}_3/\mu, \end{aligned} \quad (22)$$

---

**Algorithm 1** Procedures of implementing ELMSC
 

---

**Input:** Multi-view data matrices  $\{\mathbf{X}^{(1)}, \dots, \mathbf{X}^{(v)}\}$ , parameter  $\lambda$  and the dimension  $k$  of  $\mathbf{H}_a$ .

**Initialize:** Initialize  $\mathbf{H}_a$  using the standard Gaussian distribution;  $\mathbf{P} = \mathbf{0}$ ,  $\mathbf{E}_1 = \mathbf{0}$ ,  $\mathbf{E}_2 = \mathbf{0}$ ,  $\mathbf{Z}_a = \mathbf{J} = \mathbf{0}$ ,  $\mathbf{Y}_1 = \mathbf{0}$ ,  $\mathbf{Y}_2 = \mathbf{0}$ ,  $\mathbf{Y}_3 = \mathbf{0}$ ,  $\mu = 10^{-4}$ ,  $\mu_{max} = 10^6$ ,  $\rho = 1.2$ ,  $tol = 10^{-3}$ ,  $t = 0$ ,  $T = 100$ .

- 1: Calculate  $\mathbf{X}_a$  according to (4)-(6).
- 2: **while** not converged and  $t < T$  **do**
- 3: Update variables  $\mathbf{P}$ ,  $\mathbf{H}_a$ ,  $\mathbf{Z}_a$ ,  $\mathbf{E}$ ,  $\mathbf{J}$  according to *subproblems 1-5*.
- 4: Update multipliers  $\mathbf{Y}_1$ ,  $\mathbf{Y}_2$ ,  $\mathbf{Y}_3$  according to *subproblem 6*.
- 5: Update  $\mu$  by  $\mu = \min(\rho\mu, \mu_{max})$ .
- 6: **if**  $\|\mathbf{X}_a - \mathbf{P}\mathbf{H}_a - \mathbf{E}_1\|_\infty < tol$  and  $\|\mathbf{H}_a - \mathbf{H}_a\mathbf{Z}_a - \mathbf{E}_2\|_\infty < tol$  and  $\|\mathbf{J} - \mathbf{Z}_a\|_\infty < tol$  **then**
- 7:     Converged.
- 8:     **end if**
- 9:      $t \leftarrow t + 1$ .
- 10: **end while**

**Output:**  $\mathbf{Z}_a$ ,  $\mathbf{H}_a$ ,  $\mathbf{P}$ ,  $\mathbf{E}$

---

where  $\text{blkdiag}(\cdot)$  takes the diagonal blocks of a matrix, and  $\mathcal{T}(\cdot)$  is the shrinkage-thresholding operator acting on each element of a given matrix for solving sparse problem, defined by

$$\mathcal{T}_\eta(\gamma) = (|\gamma| - \eta)_+ \text{sgn}(\gamma). \quad (23)$$

### 6) Updating multipliers

By applying the gradient ascent operation, we update the Lagrange multipliers as

$$\begin{cases} \mathbf{Y}_1 = \mathbf{Y}_1 + \mu(\mathbf{X}_a - \mathbf{P}\mathbf{H}_a - \mathbf{E}_1) \\ \mathbf{Y}_2 = \mathbf{Y}_2 + \mu(\mathbf{H}_a - \mathbf{H}_a\mathbf{Z}_a - \mathbf{E}_2) \\ \mathbf{Y}_3 = \mathbf{Y}_3 + \mu(\mathbf{J} - \mathbf{Z}_a) \end{cases} \quad (24)$$

where  $\mu = \min(\rho\mu, \mu_{max})$  with  $\rho$  being a constant. The procedures of implementing ELMSC are summarized in Algorithm 1.

**Remark 2:** It should be noted that in contrast to the conventional self-representation matrix of dimensions  $n \times n$ , the augmented self-representation matrix denoted as  $\mathbf{Z}_a$  in our proposed ELMSC, has dimensions of  $vn \times vn$ . As a result, it is not feasible to directly utilize  $\mathbf{Z}_a$  to calculate the affinity matrix. Given that  $\mathbf{Z}_a$  comprises  $v^2$  individual block matrices, we arrive at the final self-representation matrix by accumulating all these block matrices. This procedure can be expressed as:

$$\hat{\mathbf{Z}} = \sum_i^v \sum_j^v \mathbf{Z}_a(i, j), \quad (25)$$

where  $\mathbf{Z}_a(i, j)$  denotes the  $(i, j)$ -th block matrix.

It is justifiable to use (25) for calculating the final self-representation matrix, the rationale for which is provided below. Recall that we impose sparse regularization on non-diagonal blocks. Besides its primary purpose in circumventing

redundant computations, this regularization serves an additional purpose: it encourages sparsity, indicating limited contributions from non-diagonal blocks. This implies that our design assigns higher importance to diagonal blocks and lesser to non-diagonal blocks, actually reflecting the contribution weights of each block.

Based on the resulted  $\hat{\mathbf{Z}}$ , one can perform spectral clustering to obtain the final clustering results.

### D. Computational Complexity

Our method mainly consists of two stages: 1) construction of  $\mathbf{X}_a$ ; 2) updates of various subproblems. In the first stage, we require to calculate (5) and (6), which takes a complexity of  $O(v^2n^2d)$ . In the second stage, we need to update subproblems 1-6. Specifically, the update for  $\mathbf{P}$  involves the calculation of  $\mathbf{H}_a(\mathbf{Y}_1/\mu + \mathbf{X}_a - \mathbf{E}_1)$ , the execution of SVD on the resulting matrix, and the computation of  $\mathbf{U}\mathbf{V}^T$ , which in total consumes  $O(kd^2 + kvnd)$ . The update for  $\mathbf{H}_a$  incorporates the updates of  $\mathbf{A}$ ,  $\mathbf{B}$  and  $\mathbf{C}$ , as well as solving a Sylvester equation. The total complexity for this is  $O((vn)^3 + k^3 + k^2d + kdv n)$ . The update for  $\mathbf{Z}_a$  has a complexity of  $O((vn)^3 + (vn)^2k)$ . Finally, the updates for  $\mathbf{E}$  and  $\mathbf{J}$  have complexities of  $O(dkvn + k(vn)^2)$  and  $O((vn)^2)$ , respectively.

In summary, the overall complexity is  $O(v^2n^2d + v^3n^3 + v^2n^2k + kdv n + v^2n^2 + d^2k + k^3)$ . Generally, the conditions  $k \ll d$ ,  $v \ll n$  and  $d \ll n$  hold true. Therefore, the approximate complexity can be regarded as  $O(v^3n^3)$ , which preserves the complexity order of  $O(n^3)$  that is comparable to many prevalent tensor-based multi-view methods [40], [41].

## IV. CONNECTION BETWEEN LMSC AND OUR METHOD

In contrast to LMSC, our method innovatively introduces an enhanced data reconstruction strategy, which particularly emphasizes the correlation matrix  $\mathbf{X}^{(p,q)}$  between two different views. Despite the existence of a clear distinction between LMSC and our method, we can establish the relationship between them by performing the following discussion.

If we replace the cosine similarity matrix  $\mathbf{S}^{(p,q)}$  with an identity matrix, the augmented data matrix  $\mathbf{X}_a$  is transformed into

$$\mathbf{X}_a = \begin{bmatrix} \mathbf{X}^{(1)}, & \dots, & \mathbf{X}^{(1)} \\ \mathbf{X}^{(2)}, & \dots, & \mathbf{X}^{(2)} \\ \vdots & \vdots & \vdots \\ \mathbf{X}^{(v)}, & \dots, & \mathbf{X}^{(v)} \end{bmatrix}. \quad (26)$$

Given that  $\mathbf{X}_a = \mathbf{P}\mathbf{H}_a + \mathbf{E}_1$ , we have the following equation by ignoring the error matrix  $\mathbf{E}_1$

$$\begin{bmatrix} \mathbf{X}^{(1)}, & \dots, & \mathbf{X}^{(1)} \\ \mathbf{X}^{(2)}, & \dots, & \mathbf{X}^{(2)} \\ \vdots & \vdots & \vdots \\ \mathbf{X}^{(v)} & \dots, & \mathbf{X}^{(v)} \end{bmatrix} = \begin{bmatrix} \mathbf{P}^{(1)} \\ \vdots \\ \mathbf{P}^{(v)} \end{bmatrix} [\mathbf{H}^{(1)}, \dots, \mathbf{H}^{(v)}]. \quad (27)$$

which consequently results in  $\mathbf{H}^{(1)} = \dots = \mathbf{H}^{(v)}$ .

It is noted that in our objective function, we enforce a sparse regularization on the non-diagonal blocks of  $\mathbf{Z}_a$ , denoted as

$\|\mathbf{Z}_a - \text{diag}(\mathbf{Z}_a)\|_1$ . Assuming this sparse regularization is strictly satisfied, that is,

$$\mathbf{Z}_a = \begin{bmatrix} \mathbf{Z}^{(1)}, & \cdots, & \mathbf{0} \\ \mathbf{0}, & \cdots, & \mathbf{0} \\ \vdots & \vdots & \vdots \\ \mathbf{0}, & \cdots, & \mathbf{Z}^{(v)} \end{bmatrix}, \quad (28)$$

and since  $\mathbf{H}_a = \mathbf{H}_a \mathbf{Z}_a + \mathbf{E}_2$ , we have the following result by ignoring the error matrix  $\mathbf{E}_2$

$$\begin{bmatrix} \mathbf{H}^{(1)}, & \cdots, & \mathbf{H}^{(v)} \end{bmatrix} = \begin{bmatrix} \mathbf{H}^{(1)}, & \cdots, & \mathbf{H}^{(v)} \end{bmatrix} \begin{bmatrix} \mathbf{Z}^{(1)}, & \cdots, & \mathbf{0} \\ \mathbf{0}, & \cdots, & \mathbf{0} \\ \vdots & \vdots & \vdots \\ \mathbf{0}, & \cdots, & \mathbf{Z}^{(v)} \end{bmatrix}. \quad (29)$$

From (29), it is obvious that

$$\begin{cases} \mathbf{H}^{(1)} = \mathbf{H}^{(1)} \mathbf{Z}^{(1)} \\ \mathbf{H}^{(2)} = \mathbf{H}^{(2)} \mathbf{Z}^{(2)} \\ \cdots \\ \mathbf{H}^{(v)} = \mathbf{H}^{(v)} \mathbf{Z}^{(v)}. \end{cases} \quad (30)$$

Consequently, we obtain  $\mathbf{Z}^{(1)} = \mathbf{Z}^{(2)} = \cdots = \mathbf{Z}^{(v)}$ , which is consistent with the latent representation in LMSC. From the above analysis, we demonstrate that our method can be regarded as an augmented variant of LMSC. Furthermore, under specific conditions, it simplifies to LMSC.

## V. EXPERIMENTS

In this section, we conduct comprehensive experiments to evaluate the effectiveness of the proposed ELMSC algorithm. Specifically, the clustering performance compared with other methods, affinity matrix and convergence analysis, parameter sensitivity analysis, and data visualization are conducted to perform the validation. The version of Matlab utilized is Matlab R2023a. All results are obtained by averaging 10 trials. The source code will be released on <https://github.com/caolei2000/ELMSC-Code> soon.

### A. Experimental Settings

1) *Datasets*: We select six real-world multi-view datasets, including **ORL** [28], **MSRCV1** [42], **HW** [43], **Reuters** [44], **Yale** [45], [41] and **BBCSport** [46]. Fig. 2 shows some examples of the selected datasets, and a brief description on these datasets is given below:

**ORL**<sup>1</sup>: It comprises 400 facial images from 40 subjects, each represented by 10 images. The subject label serves as the definitive class label. Images were captured under varying conditions, including lighting, time, and facial expressions or details. Three types of features are utilized: intensity, LBP, and Gabor.

**MSRCV1**<sup>2</sup>: It is composed of 210 images for scene recognition, distributed across seven categories. Each image is

characterized by six different feature sets: LBP with 256 dimensions, HOG with 100 dimensions, GIST with 512 dimensions, Color Moment with 48 dimensions, CENTRIST with 1302 dimensions, and SIFT with 210 dimensions.

**HW**<sup>3</sup>: It is composed of 2,000 data points for digits 0 to 9 from UCI machine learning repository and two public features are available.

**Reuters**<sup>4</sup>: It is a dataset of newswire articles available in five languages: French, Italian, English, German, and Spanish. Our experiment is conducted on a subset comprising 600 documents from 6 articles.

**Yale**<sup>5</sup>: It consists of 165 gray-scale images of 15 individuals with different facial expressions and configurations. Motivated by [47], 4096 dimensions intensity feature, 3304 LBP feature and 6750 dimensions Gabor feature are extracted as three multi-view features.

**BBCSport**<sup>6</sup>: It comprises 544 documents sourced from the BBC Sport website, covering news from five different categories - business, entertainment, politics, sport, and tech. These categories serve as the ground-truth class labels. In the experiments, two views with dimensions of 3183 and 3203 are selected.

2) *Compared Methods*: We compare our method with some baseline methods including: **LRR**<sub>BestSV</sub> [6], **Co-reg** [13], **AWP** [18], **MLRSSC** [27], **MCGC** [16], **CSMSC** [28], **MCLES** [31], **LMSC** [30], **TBGL** [48], **LTBPL** [47], **WTSNM** [41] and **MCLGF** [49]. The compared methods are detailed below:

**LRR**<sub>BestSV</sub>: This method employs the nuclear norm to construct the representation matrix, a technique used in single-view clustering.

**Co-reg**: This method constructs an optimal consensus adjacency matrix and uses the nuclear norm to project data into a low-dimensional subspace.

**AWP**: This method introduces an adaptively weighted procrustes strategy that weighs views based on their clustering capacities.

**MLRSSC**: This method incorporates sparsity and low-rankness to learn the representation matrix.

**MCGC**: This method learns a consensus graph by minimizing disagreement between different views and constraining the rank of the Laplacian matrix.

**CSMSC**: This method takes into account consistency and specificity jointly for subspace representation learning.

**MCLES**: This method clusters multi-view data in a learned latent embedding space.

**LMSC**: This method proposes a latent representation scheme to exploit comprehensive information from multiple views.

**TBGL**: This method uses a variance-based de-correlation anchor selection strategy for bipartite construction.

**LTBPL**: This method proposes a framework to simultaneously consider the low-rank probability affinity matrices and the integrated consensus indicator graph.

<sup>3</sup><https://cs.nyu.edu/~roweis/data.html>

<sup>4</sup><http://lig-membres.imag.fr/grimal/data.html>

<sup>5</sup><http://cvc.yale.edu/projects/yalefacesB/yalefacesB.html>

<sup>6</sup><http://mlg.ucd.ie/datasets/bbc.html>

<sup>1</sup><https://www.cl.cam.ac.uk/research/dtg/attarchive/facedatabase.html>

<sup>2</sup><http://research.microsoft.com/en-us/projects/objectclassrecognition>



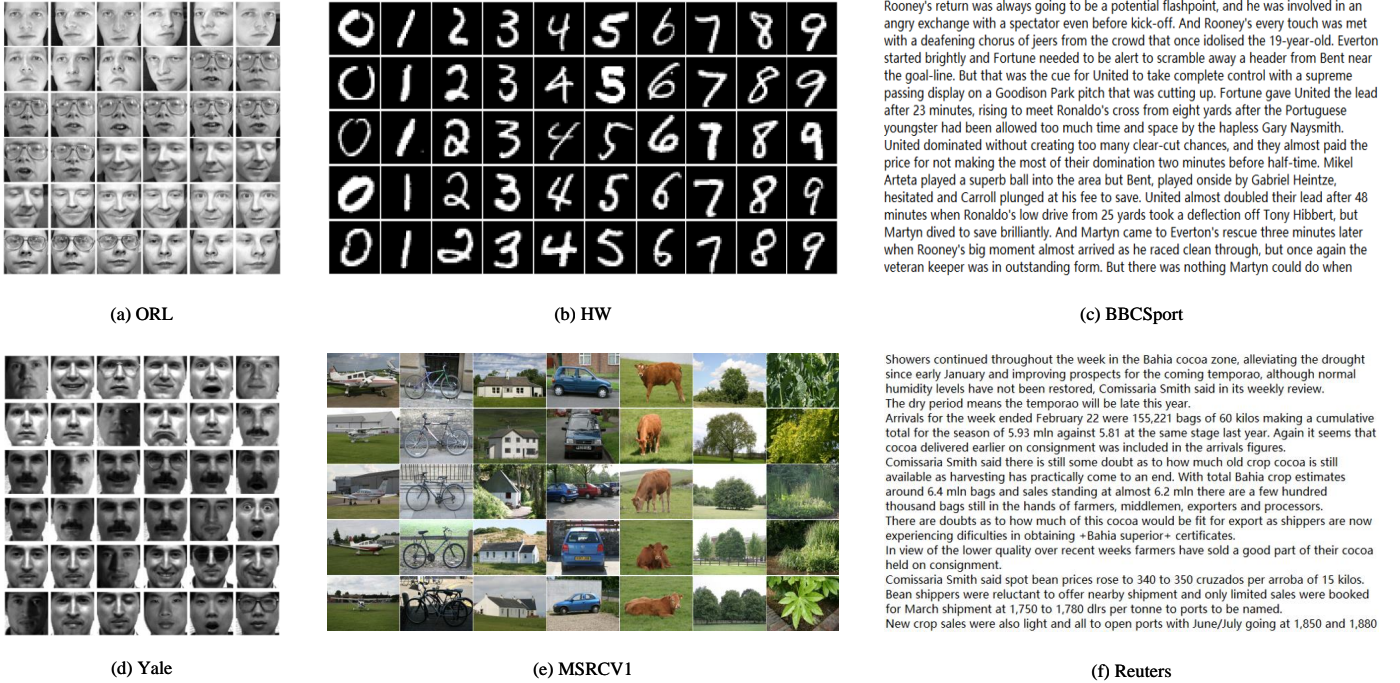


Fig. 2: Examples of the tested datasets.

**WTSNM:** This method investigates the weighted tensor Schatten  $p$ -norm to exploit the significance of different singular values in tensor-singular value decomposition.

**MCLGF:** This method constructs a consensus graph filter by considering the information across different views.

3) *Evaluation Metrics and Parameter Settings:* We evaluate the performance of all compared multi-view clustering algorithms using four widely used metrics: clustering accuracy (ACC), normalized mutual information (NMI), adjusted rand index (AR), and F1 score. For a fair comparison, the associated regularization parameters of all methods are carefully tuned over the range  $[10^{-3}, 10^3]$  with a grid size  $\{10^{-3}, 10^{-2}, 10^{-1}, 10^0, 10^1, 10^2, 10^3\}$  to achieve optimal performance.

4) *Implementation of PCA:* As mentioned below (6), our method needs to perform PCA for data samples to align dimensions. For implementing PCA, we reduce the data dimensionality across various views to a consistent  $d$  ( $d < \min(d_i, d_j)$ ). The determination of the number of principal components is influenced by the number of clusters. More specifically, we set the number of principal components to be  $clusters \times 6$ . Generally,  $clusters \times 6$  does not exceed the number of samples  $n$ . Thus, the number of principal components meets the requirement of being within the range of 0 and  $\min(n, d_i)$ . We have tested that this strategy remains about 92% ~ 98% information.

## B. Experimental Results

1) *Clustering Analysis:* Tables I and II record the clustering results of all involved multi-view clustering methods on different datasets. In the tables, we use red font to indicate the highest performance, blue font to indicate

Rooney's return was always going to be a potential flashpoint, and he was involved in an angry exchange with a spectator even before kick-off. And Rooney's every touch was met with a deafening chorus of jeers from the crowd that once idolised the 19-year-old. Everton started brightly and Fortune needed to be alert to scramble away a header from Bent near the goal-line. But that was the cue for United to take complete control with a supreme passing display on a Goodison Park pitch that was cutting up. Fortune gave United the lead after 23 minutes, rising to meet Ronaldo's cross from eight yards after the Portuguese youngster had been allowed too much time and space by the hapless Gary Naysmith. United dominated without creating too many clear-cut chances, and they almost paid the price for not making the most of their domination two minutes before half-time. Mikel Arteta played a superb ball into the area but Bent, played inside by Gabriel Heinze, hesitated and Carroll plunged at his fee to save. United almost doubled their lead after 48 minutes when Ronaldo's low drive from 25 yards took a deflection off Tony Hibbert, but Martyn dived to save brilliantly. And Martyn came to Everton's rescue three minutes later when Rooney's big moment almost arrived as he raced clean through, but once again the veteran keeper was in outstanding form. But there was nothing Martyn could do when

Showers continued throughout the week in the Bahia cocoa zone, alleviating the drought since early January and improving prospects for the coming temporoa, although normal humidity levels have not been restored, Comissaria Smith said in its weekly review. The dry period means the temporoa will be late this year. Arrivals for the week ended February 22 were 155,221 bags of 60 kilos making a cumulative total for the season of 5.93 mln against 5.81 at the same stage last year. Again it seems that cocoa delivered earlier on consignment was included in the arrivals figures. Comissaria Smith said there is still some doubt as to how much old crop cocoa is still available as harvesting has practically come to an end. With total Bahia crop estimates around 6.4 mln bags and sales standing at almost 6.2 mln there are a few hundred thousand bags still in the hands of farmers, middlemen, exporters and processors. There are doubts as to how much of this cocoa would be fit for export as shippers are now experiencing difficulties in obtaining +Bahia superior+ certificates. In view of the lower quality over recent weeks farmers have sold a good part of their cocoa held on consignment. Comissaria Smith said spot bean prices rose to 340 to 350 cruzados per arroba of 15 kilos. Bean shippers were reluctant to offer nearby shipment and only limited sales were booked for March shipment at 1,750 to 1,780 dlrs per tonne to ports to be named. New crop sales were also light and all to open ports with June/July going at 1,850 and 1,880

the second best performance, and underline font to indicate the third best performance. Note that we include two sets of results from our method in the tables, labeled as “Ours” and “Ours(random)”, where the results for “Ours” are obtained by selecting optimal regularization parameter according to the previously mentioned parameter settings, while the results for “Ours(random)” are obtained by randomly selecting regularization parameter from the grid set  $\{10^{-3}, 10^{-2}, 10^{-1}, 10^0, 10^1, 10^2, 10^3\}$ . Beside choosing the regularization parameter  $\lambda$ , our method also involves  $k$ , representing the dimensionality of latent representation, is optimally selected from the grid set  $\{50, 100, 150, 200\}$  for “Ours”, and randomly selected from the same set for “Ours(random)”.

It is seen that  $LRR_{BestSV}$ , a representative single-view clustering method, is generally inferior to all other multi-view methods in the comparison. This demonstrates the advantages of multi-view methods, which are capable of exploiting comprehensive information. We also observe that among previous methods, tensor-based methods, namely TBGL, LTBPL and WTSNM, generally provide more superior clustering performance. This suggests that tensor-based methods possess a more potent capability for data representation.

In all experiments conducted across various datasets, our proposed ELMSC algorithm with optimal parameter selection consistently shows remarkable advancement over the competing baselines in terms of all performance metrics. The only exception is the AR metric, where it ranks second on the Yale dataset. For instance, our method with optimal parameter selection yields an improvement of 6.25% in terms of ACC when contrasted with WTSNM which achieves the highest performance among previous methods. Similarly, it shows an improvement of 2.71% in terms of NMI when compared to LTBPL, another top-performing method from previous studies.

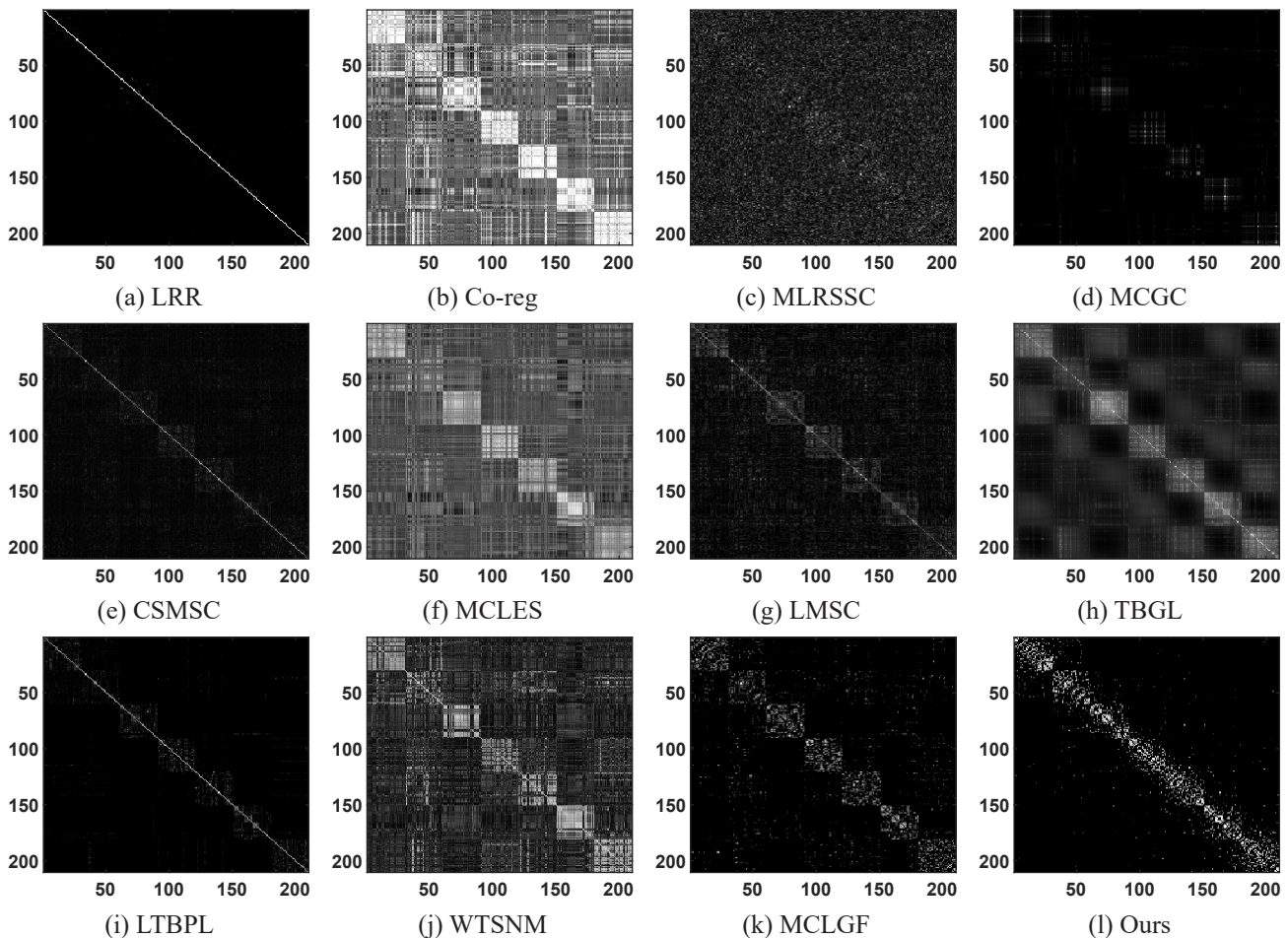


Fig. 3: Visualization of affinity matrix on MSRCV1.

Additionally, it is seen that our method with random parameter selection shows performance that is second only to that of our method with optimal parameter selection on the ORL, MSRCV1, Reuters datasets. It outperforms all other methods in terms of ACC and NMI. For example, when compared to TBGL, which achieves the highest performance among previous methods, our method with random parameter selection shows improvements of 0.33% and 0.72% in terms of ACC and NMI, respectively. Even on other datasets, our method with random parameter selection yields performance that is comparable to the best-performing method among previous ones. For instance, our method with random parameter selection achieves an ACC 57.28% that is very close to the 57.50% achieved by the top-performing previous method, LTBPL. This illustrates that our method’s performance is robust to parameter selection, demonstrating its reliability and generalizability in real-world scenarios. This advantage will be further verified in the forthcoming visualization of the parameter sensitivity analysis.

2) *Affinity Matrix and Convergence Analysis:* Fig. 3 shows the visualization results of the affinity matrix of various methods on MSRCV1. Compared with other methods, we can observe a clearer block-diagonal structure in the affinity matrix when using our method. It implies that the data samples can be effectively partitioned into distinct clusters.

Fig. 4 shows the evolutionary curves of the objective function value of ELMSC on the ORL, MSRCV1, HW, Reuters, Yale and BBCSport datasets, which empirically illustrates that the iterative algorithm in ELMSC is convergent.

3) *Parameter Sensitivity Analysis:* For conducting the parameter sensitivity analysis, we investigate the performance of our method with respect to the regularization parameter  $\lambda$  and the dimensionality of latent representation  $k$ . Fig. 5 shows the visualization results of parameter sensitivity on four datasets. Our method consistently achieves stable performance for different parameters in terms of all performance metrics. An exception is observed with the HW dataset, where our proposed method experiences minor fluctuations with different choices of  $k$ . Overall, our method’s performance is not significantly sensitive to parameter selection. Therefore, even when our method operates with randomly selected parameters, it is expected to yield a satisfactory performance that closely approximates the optimal performance.

4) *Visualization of Clustering Results:* In order to visualize more intuitively, we present the t-Distributed Stochastic Neighbor Embedding (T-SNE) [50] visualization results of nine methods, as show in Fig. 6. It is observed that tensor-based multi-view methods typically yield superior cluster partitions compared to other techniques. For instance, LTBPL demonstrates a distinct partition result, whereas CSMSC presents lit-



TABLE I: Evaluation metrics of multi-view clustering algorithms on ORL, MSRCV1 and HW (%). Red font indicates the highest performance, blue font indicates the second best performance, and underline font indicates the third best performance.

Datasets	Method	ACC	NMI	AR	F1
ORL	LRR <sub>BestSV</sub>	74.70 ± 1.91	92.50 ± 0.70	68.60 ± 3.15	69.44 ± 3.05
	Co-reg	81.50 ± 1.67	90.22 ± 0.53	74.15 ± 1.67	74.76 ± 1.63
	AWP	79.25 ± 0.00	90.11 ± 0.00	73.31 ± 0.00	73.95 ± 0.00
	MLRSSC	73.53 ± 1.10	85.57 ± 0.71	62.60 ± 1.28	63.50 ± 1.25
	MCGC	73.00 ± 0.00	86.86 ± 0.00	62.09 ± 0.00	63.04 ± 0.00
	CSMSC	81.30 ± 2.06	92.54 ± 0.75	76.27 ± 2.24	76.85 ± 2.18
	MCLES	79.65 ± 2.51	90.75 ± 1.35	69.47 ± 3.71	70.25 ± 3.59
	LMSC	83.25 ± 1.81	92.77 ± 0.46	<u>77.41 ± 1.53</u>	<u>77.95 ± 1.49</u>
	TBGL	73.50 ± 0.00	85.56 ± 0.00	<u>31.96 ± 0.00</u>	<u>34.38 ± 0.00</u>
	LTBPL	81.75 ± 0.00	<u>93.72 ± 0.00</u>	61.54 ± 0.00	62.67 ± 0.00
	WTSNM	84.25 ± 0.00	<u>91.17 ± 0.00</u>	76.10 ± 0.00	76.66 ± 0.00
	MCLGF	<u>82.75 ± 0.00</u>	88.93 ± 0.00	72.70 ± 0.00	73.32 ± 0.00
	<b>Ours</b>	<b>90.50 ± 1.57</b>	<b>96.43 ± 0.56</b>	<b>88.31 ± 1.63</b>	<b>88.59 ± 1.60</b>
	<b>Ours(random)</b>	<b>85.88 ± 1.67</b>	<b>95.53 ± 0.44</b>	<b>83.54 ± 1.29</b>	<b>83.93 ± 1.26</b>
MSRCV1	LRR <sub>BestSV</sub>	62.86 ± 0.00	55.23 ± 0.00	44.28 ± 0.00	53.09 ± 0.00
	Co-reg	80.71 ± 0.25	72.85 ± 0.63	64.92 ± 0.53	69.88 ± 0.45
	AWP	75.24 ± 0.00	72.00 ± 0.00	62.75 ± 0.00	68.66 ± 0.00
	MLRSSC	29.76 ± 0.79	11.70 ± 0.37	4.77 ± 0.33	18.28 ± 0.27
	MCGC	74.76 ± 0.00	67.89 ± 0.00	59.97 ± 0.00	65.88 ± 0.00
	CSMSC	85.86 ± 0.60	76.54 ± 0.87	70.98 ± 1.07	75.06 ± 0.91
	MCLES	84.57 ± 6.79	80.52 ± 2.73	72.58 ± 5.46	76.55 ± 4.55
	LMSC	77.76 ± 2.79	69.79 ± 3.51	62.63 ± 5.02	67.94 ± 4.33
	TBGL	<u>98.10 ± 0.00</u>	<u>96.03 ± 0.00</u>	95.54 ± 0.00	96.16 ± 0.00
	LTBPL	<u>97.52 ± 0.00</u>	<u>97.92 ± 0.00</u>	<b>97.88 ± 0.00</b>	<b>98.03 ± 0.00</b>
	WTSNM	80.00 ± 0.00	67.31 ± 0.00	59.94 ± 0.00	65.60 ± 0.00
	MCLGF	88.57 ± 0.00	80.60 ± 0.00	75.84 ± 0.00	79.24 ± 0.00
	<b>Ours</b>	<b>98.57 ± 0.78</b>	<b>97.03 ± 1.38</b>	<b>96.68 ± 1.75</b>	<b>97.14 ± 1.51</b>
	<b>Ours(random)</b>	<b>98.43 ± 0.39</b>	<b>96.75 ± 0.70</b>	96.33 ± 0.89	96.84 ± 0.77
HW	LRR <sub>BestSV</sub>	45.42 ± 0.31	40.64 ± 0.17	27.05 ± 0.23	34.76 ± 0.20
	Co-reg	72.29 ± 0.71	74.86 ± 1.00	63.81 ± 1.13	67.54 ± 1.03
	AWP	69.85 ± 0.00	75.76 ± 0.00	61.59 ± 0.00	65.73 ± 0.00
	MLRSSC	53.55 ± 0.30	46.95 ± 0.27	36.54 ± 0.16	43.13 ± 0.14
	MCGC	68.90 ± 0.00	66.84 ± 0.00	56.53 ± 0.00	61.16 ± 0.00
	CSMSC	89.79 ± 0.99	82.66 ± 0.65	79.81 ± 1.37	81.83 ± 1.23
	MCLES	82.68 ± 0.10	88.93 ± 0.19	80.41 ± 0.11	82.51 ± 0.10
	LMSC	80.33 ± 3.60	79.02 ± 2.07	71.88 ± 3.38	74.78 ± 3.01
	TBGL	98.05 ± 0.00	96.04 ± 0.00	95.54 ± 0.00	95.98 ± 0.00
	LTBPL	<b>99.55 ± 0.00</b>	<b>98.83 ± 0.00</b>	<b>99.00 ± 0.00</b>	<b>99.10 ± 0.00</b>
	WTSNM	65.65 ± 0.00	58.04 ± 0.00	50.40 ± 0.00	55.39 ± 0.00
	MCLGF	<u>98.60 ± 0.00</u>	<u>96.69 ± 0.00</u>	<u>96.92 ± 0.00</u>	<u>97.23 ± 0.00</u>
	<b>Ours</b>	<b>99.82 ± 0.03</b>	<b>99.59 ± 0.08</b>	<b>99.59 ± 0.07</b>	<b>99.63 ± 0.07</b>
	<b>Our(random)</b>	88.11 ± 4.39	95.33 ± 1.64	88.80 ± 3.70	90.00 ± 3.26

the messy partitions. Furthermore, in contrast with the previous methods, our method achieves the distinction of clusters in a more discriminative and clear manner.

## VI. CONCLUSIONS

In this paper, we propose a novel latent multi-view subspace clustering method, namely ELMSC. In ELMSC, we construct an augmented multi-view data matrix, in which the diagonal blocks stack data matrices from each view for preserving complementary information, while the non-diagonal blocks comprise of the similarity information between different views

to ensure consistency. This data construction strategy significantly contributes to a more comprehensive recovery of latent representations. In addition, we enforce a sparse regularization for the non-diagonal blocks of the augmented self-representation matrix, mitigating redundant computations of consistent information. Meanwhile, we devise a novel iterative algorithm using ADMM for ELMSC. Furthermore, we establish the relationship between LMSC and our method. Experiment results on real-world datasets validate the advantages of ELMSC over several established baselines.

TABLE II: Evaluation metrics of multi-view clustering algorithms on Reuters, Yale and BBCSport (%). Red font indicates the highest performance, blue font indicates the second best performance, and underline font indicates the third best performance.

Datasets	Method	ACC	NMI	AR	F1
Reuters	LRR <sub>BestSV</sub>	22.17 ± 0.61	1.85 ± 0.90	0.18 ± 0.19	17.02 ± 0.48
	Co-reg	24.50 ± 0.00	20.99 ± 0.19	2.64 ± 0.01	29.03 ± 0.02
	AWP	24.33 ± 0.00	21.42 ± 0.00	2.61 ± 0.00	29.05 ± 0.00
	MLRSSC	42.37 ± 0.46	25.77 ± 0.35	13.91 ± 0.55	31.71 ± 0.12
	MCGC	31.67 ± 0.00	25.10 ± 0.00	4.31 ± 0.00	28.94 ± 0.00
	CSMSC	50.43 ± 0.41	32.71 ± 0.41	22.88 ± 0.25	36.60 ± 0.26
	MCLES	36.82 ± 5.17	33.13 ± 4.82	12.88 ± 3.89	34.51 ± 2.03
	LMSC	37.03 ± 1.28	26.42 ± 1.28	12.43 ± 1.19	31.87 ± 0.79
	TBGL	21.33 ± 0.00	12.65 ± 0.00	0.68 ± 0.00	28.22 ± 0.00
	LTBPL	<u>57.50 ± 0.00</u>	<u>49.66 ± 0.00</u>	<u>31.79 ± 0.00</u>	<u>47.06 ± 0.00</u>
	WTSNM	55.00 ± 0.00	15.15 ± 0.00	10.99 ± 0.00	25.76 ± 0.00
	MCLGF	50.50 ± 0.00	37.52 ± 0.00	26.79 ± 0.00	40.89 ± 0.00
	<b>Ours</b>	<b>57.95 ± 1.32</b>	<b>67.11 ± 1.23</b>	<b>48.75 ± 0.78</b>	<b>59.25 ± 0.61</b>
<b>Ours(random)</b>	<b>57.28 ± 0.44</b>	<b>66.23 ± 0.56</b>	<b>48.25 ± 0.57</b>	<b>58.86 ± 0.45</b>	
Yale	LRR <sub>BestSV</sub>	64.06 ± 0.91	66.16 ± 0.55	38.64 ± 0.91	42.84 ± 0.81
	Co-reg	62.85 ± 0.76	67.16 ± 0.69	46.90 ± 1.16	50.26 ± 1.09
	AWP	63.64 ± 0.00	67.96 ± 0.00	48.51 ± 0.00	51.74 ± 0.00
	MLRSSC	67.21 ± 2.13	70.25 ± 2.19	49.38 ± 3.08	52.60 ± 2.28
	MCGC	62.42 ± 0.00	65.17 ± 0.00	44.09 ± 0.00	47.67 ± 0.00
	CSMSC	71.94 ± 2.37	72.95 ± 1.58	55.39 ± 2.57	58.22 ± 2.39
	MCLES	69.76 ± 1.35	72.90 ± 1.85	50.05 ± 3.86	53.41 ± 3.52
	LMSC	<u>74.30 ± 1.49</u>	76.81 ± 0.75	<b>59.00 ± 1.14</b>	<u>61.63 ± 1.06</u>
	TBGL	69.09 ± 0.00	72.53 ± 0.00	50.06 ± 0.00	53.47 ± 0.00
	LTBPL	69.39 ± 0.00	71.97 ± 0.00	29.93 ± 0.00	35.61 ± 0.00
	WTSNM	73.33 ± 0.00	71.86 ± 0.00	51.01 ± 0.00	54.16 ± 0.00
	MCLGF	73.94 ± 0.00	<u>77.06 ± 0.00</u>	61.09 ± 0.00	<b>63.54 ± 0.00</b>
	<b>Ours</b>	<b>76.12 ± 3.45</b>	<b>78.02 ± 2.19</b>	<b>58.34 ± 3.62</b>	61.01 ± 3.38
<b>Ours(random)</b>	<b>73.33 ± 2.73</b>	<b>76.96 ± 1.55</b>	<b>55.91 ± 3.40</b>	<b>58.77 ± 3.12</b>	
BBCSport	LRR <sub>BestSV</sub>	60.86 ± 0.06	59.16 ± 0.20	39.26 ± 0.04	59.06 ± 0.02
	Co-reg	60.29 ± 0.39	47.96 ± 0.72	34.32 ± 0.26	50.68 ± 0.18
	AWP	63.42 ± 0.00	50.07 ± 0.00	37.99 ± 0.00	56.36 ± 0.00
	MLRSSC	90.61 ± 0.06	78.02 ± 0.13	81.64 ± 0.12	85.95 ± 0.09
	MCGC	<u>97.43 ± 0.00</u>	<u>91.45 ± 0.00</u>	<u>93.76 ± 0.00</u>	<u>95.25 ± 0.00</u>
	CSMSC	95.59 ± 0.00	86.19 ± 0.00	88.82 ± 0.00	91.48 ± 0.00
	MCLES	87.98 ± 0.31	82.93 ± 1.28	84.12 ± 1.02	88.05 ± 0.76
	LMSC	86.47 ± 10.73	75.70 ± 13.03	76.77 ± 17.72	82.61 ± 12.71
	TBGL	52.02 ± 0.00	25.08 ± 0.00	13.40 ± 0.00	42.76 ± 0.00
	LTBPL	86.21 ± 0.00	79.78 ± 0.00	79.60 ± 0.00	84.78 ± 0.00
	WTSNM	50.74 ± 0.00	23.48 ± 0.00	16.72 ± 0.00	34.86 ± 0.00
	MCLGF	84.38 ± 0.00	68.95 ± 0.00	66.90 ± 0.00	75.15 ± 0.00
	<b>Ours</b>	<b>99.60 ± 0.12</b>	<b>98.49 ± 0.40</b>	<b>98.94 ± 0.35</b>	<b>99.20 ± 0.27</b>
<b>Ours(random)</b>	<b>99.52 ± 0.13</b>	<b>98.21 ± 0.48</b>	<b>98.79 ± 0.32</b>	<b>99.08 ± 0.24</b>	

## REFERENCES

- [1] R. Vidal, "Subspace clustering," *IEEE Signal Processing Magazine*, vol. 28, no. 2, pp. 52–68, 2011.
- [2] C.-G. Li, C. You, and R. Vidal, "Structured sparse subspace clustering: A joint affinity learning and subspace clustering framework," *IEEE Transactions on Image Processing*, vol. 26, no. 6, pp. 2988–3001, 2017.
- [3] L. Cao, L. Shi, J. Wang, Z. Yang, and B. Chen, "Robust subspace clustering by logarithmic hyperbolic cosine function," *IEEE Signal Processing Letters*, 2023.
- [4] E. Elhamifar and R. Vidal, "Sparse subspace clustering: Algorithm, theory, and applications," *IEEE Transactions on Pattern Analysis and Machine Intelligence*, vol. 35, no. 11, pp. 2765–2781, 2013.
- [5] S. Huang, I. Tsang, Z. Xu, J. Lv, and Q.-H. Liu, "Multi-view clustering on topological manifold," in *Proceedings of the AAAI Conference on Artificial Intelligence*, vol. 36, no. 6, 2022, pp. 6944–6951.
- [6] G. Liu, Z. Lin, S. Yan, J. Sun, Y. Yu, and Y. Ma, "Robust recovery of subspace structures by low-rank representation," *IEEE Transactions on Pattern Analysis and Machine Intelligence*, vol. 35, no. 1, pp. 171–184, 2012.
- [7] C. Lu, J. Feng, Z. Lin, T. Mei, and S. Yan, "Subspace clustering by block diagonal representation," *IEEE Transactions on Pattern Analysis and Machine Intelligence*, vol. 41, no. 2, pp. 487–501, 2018.
- [8] F. Wu, P. Yuan, G. Shi, X. Li, W. Dong, and J. Wu, "Robust subspace clustering network with dual-domain regularization," *Pattern Recognition Letters*, vol. 149, pp. 44–50, 2021.
- [9] C. Xu, D. Tao, and C. Xu, "A survey on multi-view learning," *arXiv preprint arXiv:1304.5634*, 2013.
- [10] H. Gao, F. Nie, X. Li, and H. Huang, "Multi-view subspace clustering," in *Proceedings of the AAAI Conference on Artificial Intelligence*, 2015, pp. 4238–4246.
- [11] X. Cao, C. Zhang, H. Fu, S. Liu, and H. Zhang, "Diversity-induced multi-view subspace clustering," in *Proceedings of the IEEE Conference on Computer Vision and Pattern Recognition*, 2015, pp. 586–594.
- [12] Q. Qiang, B. Zhang, F. Wang, and F. Nie, "Fast multi-view discrete clustering with anchor graphs," in *Proceedings of the AAAI Conference*

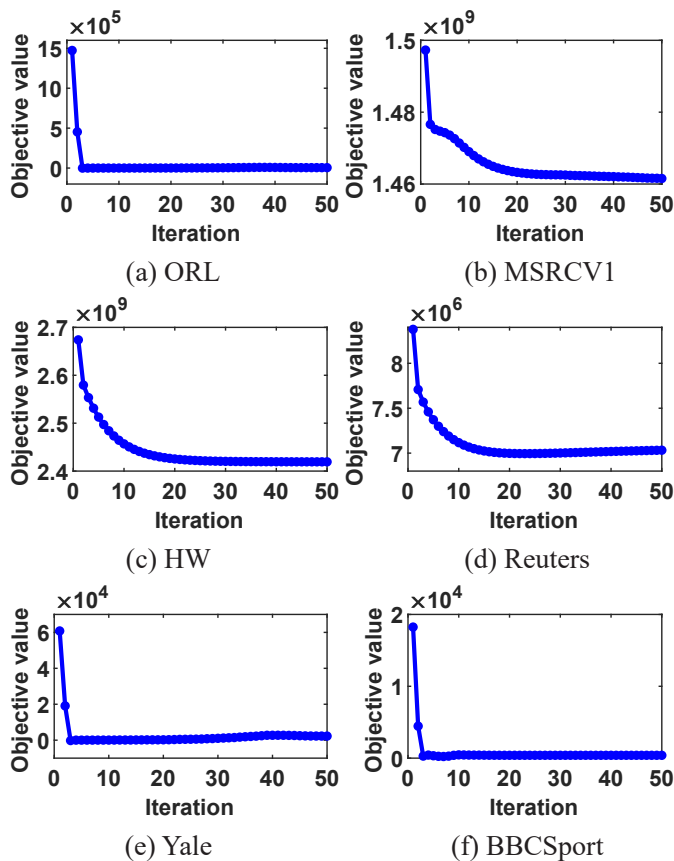


Fig. 4: Convergence of ELMSC.

- on *Artificial Intelligence*, vol. 35, no. 11, 2021, pp. 9360–9367.
- [13] A. Kumar, P. Rai, and H. Daume, “Co-regularized multi-view spectral clustering,” *Advances in Neural Information Processing Systems*, vol. 24, 2011.
- [14] Y. Li, F. Nie, H. Huang, and J. Huang, “Large-scale multi-view spectral clustering via bipartite graph,” in *Proceedings of the AAAI Conference on Artificial Intelligence*, vol. 29, no. 1, 2015.
- [15] H. Wang, Y. Yang, and B. Liu, “Gmc: Graph-based multi-view clustering,” *IEEE Transactions on Knowledge and Data Engineering*, vol. 32, no. 6, pp. 1116–1129, 2019.
- [16] K. Zhan, F. Nie, J. Wang, and Y. Yang, “Multiview consensus graph clustering,” *IEEE Transactions on Image Processing*, vol. 28, no. 3, pp. 1261–1270, 2018.
- [17] X. Zhu, S. Zhang, W. He, R. Hu, C. Lei, and P. Zhu, “One-step multi-view spectral clustering,” *IEEE Transactions on Knowledge and Data Engineering*, vol. 31, no. 10, pp. 2022–2034, 2018.
- [18] F. Nie, L. Tian, and X. Li, “Multiview clustering via adaptively weighted procrustes,” in *Proceedings of the 24th ACM SIGKDD International Conference on Knowledge Discovery & Data Mining*, 2018, pp. 2022–2030.
- [19] X. Liu, Y. Dou, J. Yin, L. Wang, and E. Zhu, “Multiple kernel k-means clustering with matrix-induced regularization,” in *Proceedings of the AAAI Conference on Artificial Intelligence*, vol. 30, no. 1, 2016.
- [20] S. Wang, X. Liu, E. Zhu, C. Tang, J. Liu, J. Hu, J. Xia, and J. Yin, “Multi-view clustering via late fusion alignment maximization,” in *International Joint Conference on Artificial Intelligence*, 2019, pp. 3778–3784.
- [21] S. Zhou, X. Liu, M. Li, E. Zhu, L. Liu, C. Zhang, and J. Yin, “Multiple kernel clustering with neighbor-kernel subspace segmentation,” *IEEE Transactions on Neural Networks and Learning Systems*, vol. 31, no. 4, pp. 1351–1362, 2019.
- [22] Z. Li, C. Tang, X. Liu, X. Zheng, W. Zhang, and E. Zhu, “Consensus graph learning for multi-view clustering,” *IEEE Transactions on Multimedia*, vol. 24, pp. 2461–2472, 2021.
- [23] Z. Lin, Z. Kang, L. Zhang, and L. Tian, “Multi-view attributed graph clustering,” *IEEE Transactions on Knowledge and Data Engineering*, 2021.
- [24] L. Li, S. Wang, X. Liu, E. Zhu, L. Shen, K. Li, and K. Li, “Local sample-weighted multiple kernel clustering with consensus discriminative graph,” *IEEE Transactions on Neural Networks and Learning Systems*, 2022.
- [25] X. Liu, “Simplemkkm: Simple multiple kernel k-means,” *IEEE Transactions on Pattern Analysis and Machine Intelligence*, vol. 45, no. 4, pp. 5174–5186, 2022.
- [26] J. Chen, H. Mao, D. Peng, C. Zhang, and X. Peng, “Multiview clustering by consensus spectral rotation fusion,” *IEEE Transactions on Image Processing*, 2023.
- [27] M. Brbić and I. Kopriva, “Multi-view low-rank sparse subspace clustering,” *Pattern Recognition*, vol. 73, pp. 247–258, 2018.
- [28] S. Luo, C. Zhang, W. Zhang, and X. Cao, “Consistent and specific multi-view subspace clustering,” in *Proceedings of the AAAI conference on Artificial Intelligence*, vol. 32, no. 1, 2018.
- [29] C. Zhang, Q. Hu, H. Fu, P. Zhu, and X. Cao, “Latent multi-view subspace clustering,” in *Proceedings of the IEEE Conference on Computer Vision and Pattern Recognition*, 2017, pp. 4279–4287.
- [30] C. Zhang, H. Fu, Q. Hu, X. Cao, Y. Xie, D. Tao, and D. Xu, “Generalized latent multi-view subspace clustering,” *IEEE Transactions on Pattern Analysis and Machine Intelligence*, vol. 42, no. 1, pp. 86–99, 2018.
- [31] M.-S. Chen, L. Huang, C.-D. Wang, and D. Huang, “Multi-view clustering in latent embedding space,” in *Proceedings of the AAAI conference on Artificial Intelligence*, vol. 34, no. 04, 2020, pp. 3513–3520.
- [32] S. Boyd, N. Parikh, E. Chu, B. Peleato, J. Eckstein *et al.*, “Distributed optimization and statistical learning via the alternating direction method of multipliers,” *Foundations and Trends® in Machine learning*, vol. 3, no. 1, pp. 1–122, 2011.
- [33] F. Nie, X. Wang, M. Jordan, and H. Huang, “The constrained laplacian rank algorithm for graph-based clustering,” in *Proceedings of the AAAI Conference on Artificial Intelligence*, vol. 30, no. 1, 2016.
- [34] Y. Tan, Y. Liu, H. Wu, J. Lv, and S. Huang, “Metric multi-view graph clustering,” in *Proceedings of the AAAI Conference on Artificial Intelligence*, vol. 37, no. 8, 2023, pp. 9962–9970.
- [35] H. Abdi and L. J. Williams, “Principal component analysis,” *Wiley Interdisciplinary Reviews: Computational Statistics*, vol. 2, no. 4, pp. 433–459, 2010.
- [36] R. Bro and A. K. Smilde, “Principal component analysis,” *Analytical methods*, vol. 6, no. 9, pp. 2812–2831, 2014.
- [37] Z. Lin, R. Liu, and Z. Su, “Linearized alternating direction method with adaptive penalty for low-rank representation,” *Advances in Neural Information Processing Systems*, vol. 24, 2011.
- [38] J. Huang, F. Nie, and H. Huang, “Spectral rotation versus k-means in spectral clustering,” in *Proceedings of the AAAI Conference on Artificial Intelligence*, vol. 27, no. 1, 2013, pp. 431–437.
- [39] J.-F. Cai, E. J. Candès, and Z. Shen, “A singular value thresholding algorithm for matrix completion,” *SIAM Journal on Optimization*, vol. 20, no. 4, pp. 1956–1982, 2010.
- [40] Y. Tang, Y. Xie, C. Zhang, and W. Zhang, “Constrained tensor representation learning for multi-view semi-supervised subspace clustering,” *IEEE Transactions on Multimedia*, vol. 24, pp. 3920–3933, 2021.
- [41] W. Xia, X. Zhang, Q. Gao, X. Shu, J. Han, and X. Gao, “Multiview subspace clustering by an enhanced tensor nuclear norm,” *IEEE Transactions on Cybernetics*, vol. 52, no. 9, pp. 8962–8975, 2021.
- [42] J. Winn and N. Jovic, “Locus: Learning object classes with unsupervised segmentation,” in *Tenth IEEE International Conference on Computer Vision*, vol. 1, 2005, pp. 756–763.
- [43] A. Asuncion and D. Newman, “Uci machine learning repository,” 2007.
- [44] C. Apté, F. Damerau, and S. M. Weiss, “Automated learning of decision rules for text categorization,” *ACM Transactions on Information Systems*, vol. 12, no. 3, pp. 233–251, 1994.
- [45] H. Wang, G. Han, B. Zhang, G. Tao, and H. Cai, “Multi-view learning a decomposable affinity matrix via tensor self-representation on grassmann manifold,” *IEEE Transactions on Image Processing*, vol. 30, pp. 8396–8409, 2021.
- [46] Y. Chen, X. Xiao, C. Peng, G. Lu, and Y. Zhou, “Low-rank tensor graph learning for multi-view subspace clustering,” *IEEE Transactions on Circuits and Systems for Video Technology*, vol. 32, no. 1, pp. 92–104, 2021.
- [47] M.-S. Chen, C.-D. Wang, and J.-H. Lai, “Low-rank tensor based proximity learning for multi-view clustering,” *IEEE Transactions on Knowledge and Data Engineering*, vol. 35, no. 5, pp. 5076–5090, 2022.
- [48] W. Xia, Q. Gao, Q. Wang, X. Gao, C. Ding, and D. Tao, “Tensorized bipartite graph learning for multi-view clustering,” *IEEE Transactions*

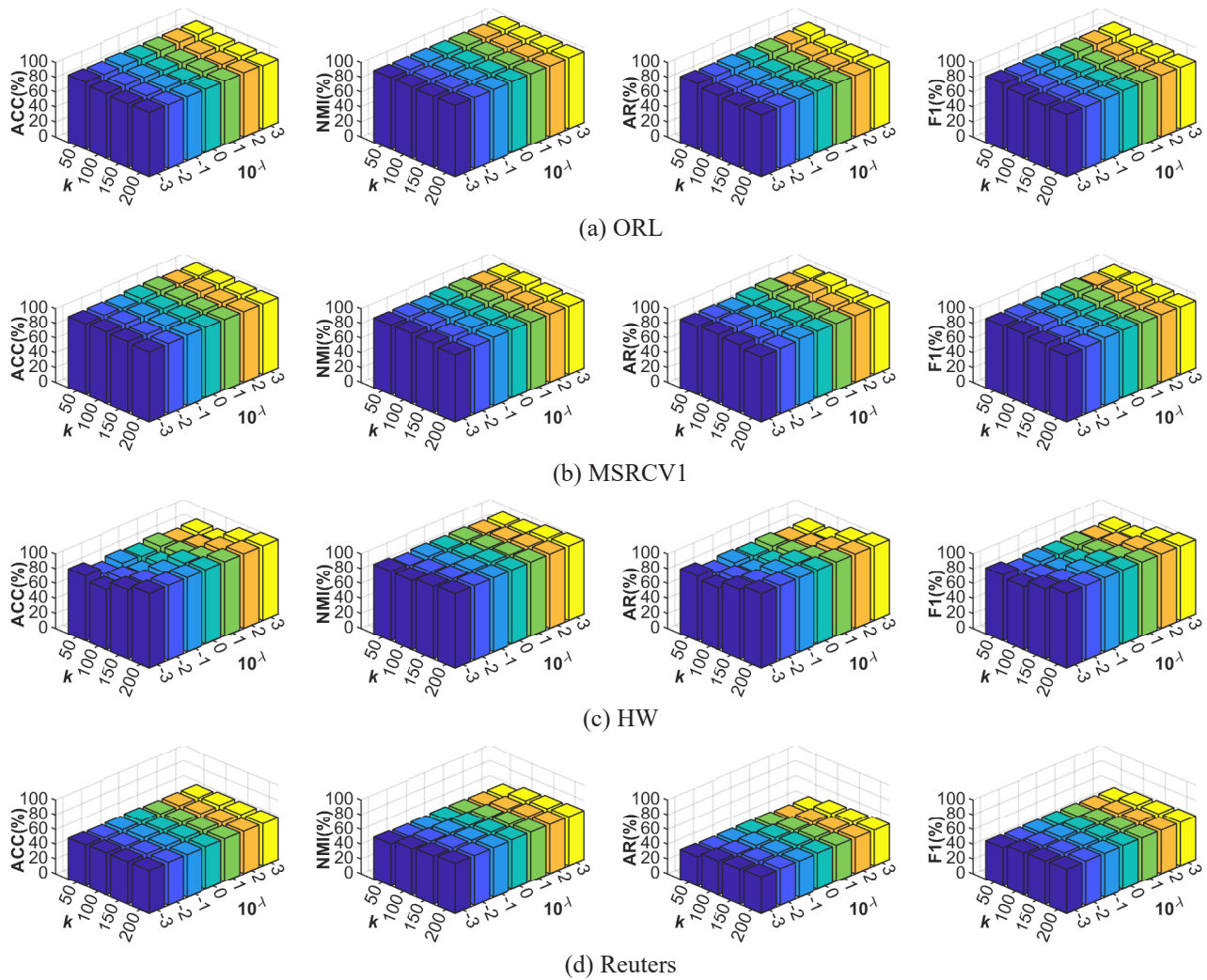


Fig. 5: Parameter sensitivity analysis of the proposed method.

on *Pattern Analysis and Machine Intelligence*, vol. 45, no. 4, pp. 5187–5202, 2022.

- [49] P. Zhou and L. Du, “Learnable graph filter for multi-view clustering,” in *Proceedings of the 31st ACM International Conference on Multimedia*, 2023, pp. 3089–3098.
- [50] L. Van der Maaten and G. Hinton, “Visualizing data using t-sne.” *Journal of Machine Learning Research*, vol. 9, no. 11, 2008.

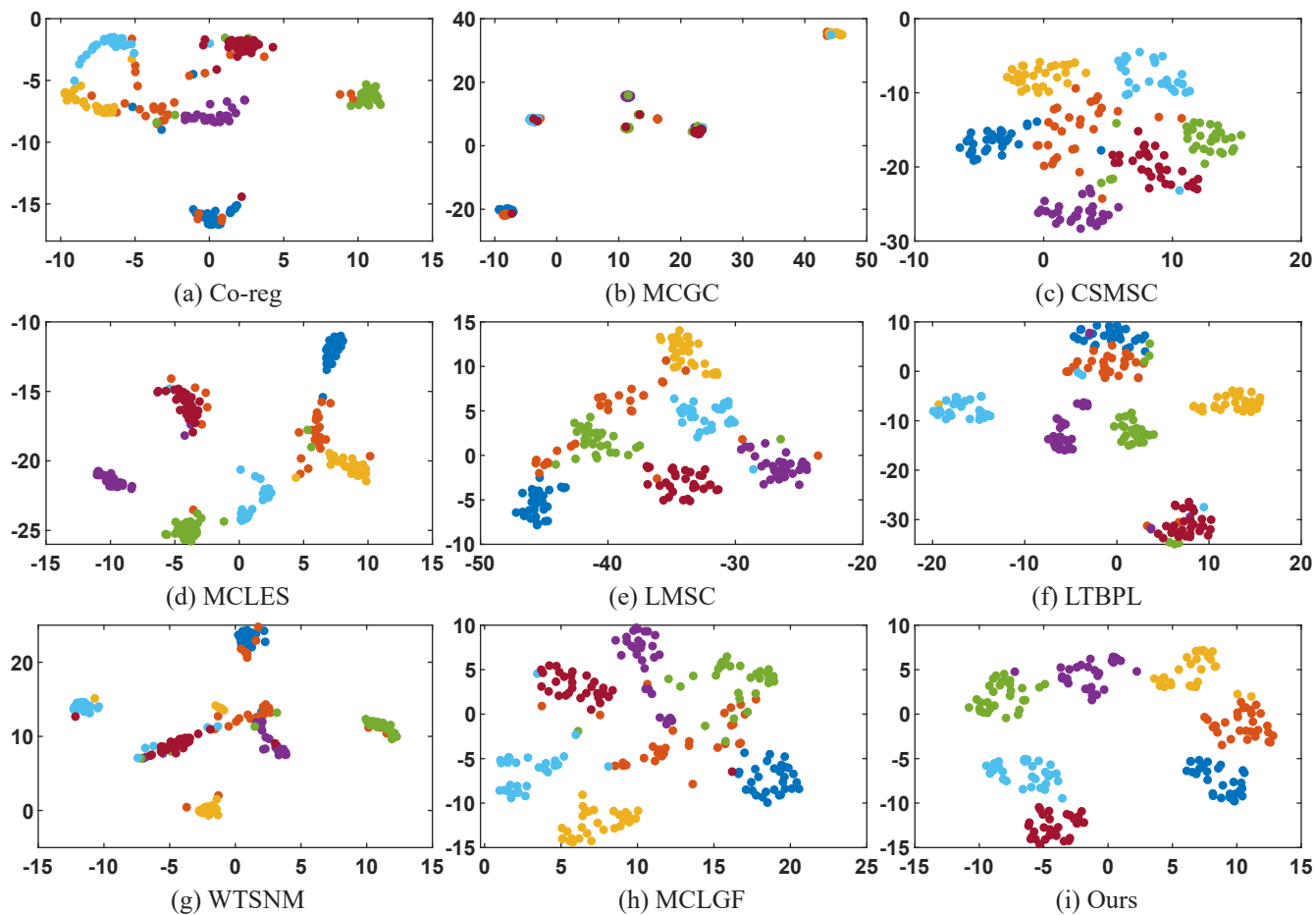


Fig. 6: T-SNE visualization of various methods on MSRCV1.